INFLUENCE OF AGGREGATE CONTENT ON THE MIGRATION BEHAVIOR OF CATIONS USING THE ACCELERATED LITHIUM MIGRATION TECHNIQUE

Chih Chien Liu [1 *], Wen Ten Kuo [2], Wei Chien Wang [3], Chia Ying Hsu [2]

[1]Department of Civil Engineering, R.O.C. Military Acadamy, Fengshan 830, Taiwan, R.O.C.

[2] Department of Civil Engineering, National Kaohsiung University of Applied Sciences, Kaohsiung 807, Taiwan, R.O.C.

[3] Department of Civil Engineering, Chung Yuan Christian University, ChungLi 32001, Taiwan, R.O.C.

Abstract

This paper researches the influence of aggregate content (V_f) in mortar on the migration behavior of cations using the Accelerated Lithium Migration Technique (ALMT). The results show that three stages for Li^+ migration can be observed during the ALMT: non-steady state, transition, and steady state. During the transitional stage, voltage reached a peak value before the complete removal of Na^+. The time required for reaching the peak value decreased with the increase in V_f, while the peak value increased with the increase in V_f. The removed proportion of the Na^+ and K^+ both decreased with the increase in V_f. When V_f was less than 20%, the Li^+ migration coefficient was influenced by the dilution effect and tortuosity effect of aggregate. The combination effect of ITZ and percolation occurs at V_f=30%, and the effects increased with the increase in V_f.

Keywords: electrochemical technique, alkali-silica reaction, migration, lithium

1 INTRODUCTION

In 1998, Chen [1] conceived of using ionic migration from electrodes to drive the Na^+ and K^+ that can induce ASR out of the concrete, while simultaneously driving in the Li^+ that can inhibit ASR. Experimentation confirmed claims that this method can remedy ASR damage. The method was then named Accelerated Lithium Migration Technique (ALMT) [2].

Cement-based materials contain air voids, capillary pores, and gel pores (the interlayer spaces in a C-S-H gel). The pores in concrete are randomly-sized, arranged, and connected [3]. The permeability of concrete is influenced by the pore size distribution and continuity. In normal concrete or mortar, the microstructure of matrix near-aggregate surface region differs from the bulk cement paste. This layer around the aggregate is called the interfacial transition zone (ITZ) [4]. The influence of aggregate in the hydrated cement paste is fourfold: dilution, tortuosity, ITZ, and percolation. The dilution and tortuosity effects reduce concrete permeability while the ITZ and percolation effects increase permeability [5].

This research was undertaken to analyze the influence of aggregate content regarding the migration behavior of cations under the ALMT. The Li^+ steady-state migration coefficient of mortars was obtained using the ALMT and the migration coefficient was used to assess the dilution, tortuosity, ITZ, and percolation effects of aggregate in cement-based composites. The cation content within the mortar related to ASR after the process was also analyzed to validate the effectiveness of the treatment.

* Correspondence to: luc5453@yahoo.com.tw

2 MATERIALS AND METHODS

2.1 Materials and specimen preparation

ASTM Type 1 Portland cement was used, the chemical compositions of the cement is listed in Table 1, with Na_2O content of 0.29% and K_2O content of 0.58%, the content of alkali transformed into Na_2O_{eq} is 0.67%. Non-ASR-active meta-sandstone from western Taiwan was used as the aggregate. The specific gravity and absorption capacity of the aggregate are 2.60 and 1.3%, respectively. The fine aggregate gradation is in agreement with the ASTM C227 specifications.

Different fine aggregate volume fractions (V_f, the volume of fine aggregate/the volume of mortar) were selected and a 0.5 w/c ratio was considered. The mixture proportions are shown in Table 2. For each mix, two cylindrical specimens (φ: 100 mm×200 mm) were cast. The specimen was demoulded the day after its fabrication and was cured in a 23°C, 100% R.H. environment for 3 months. A 3-month curing time was set to ensure the cement hydration maturation.

2.2 ALMT experiment apparatus and procedure

The ALMT electrochemical module is shown in Figure 1. A constant current density of 9 A/m^2 was applied during the ALMT, and a data logger was used to record the changes in voltage per ten minutes. The ALMT module was sealed by silicone stopper to prevent CO_2 from interacting with the catholyte during the experiment [2]. The generated gases in both the anolyte and catholyte were collected by a method using water displacement and analyzed by a residual gas analyzer (RGA) during the ALMT. An Ion Chromatograph (IC) was used to periodically analyze the cation concentrations in the catholyte.

After the mortar was cured, two 3-cm-tall specimens were cut from the mid-portion of cylindrical specimen. Specimen preparation before the electrochemical process was undertaken according to the ASTM C1202. The prepared specimens were installed in the ALMT module. The time chosen for the electrochemical process was based on how long the flux of the system's Li^+ could maintain a steady state. Therefore, except for Mixturees A0 and A1 which had a process time of 60 days, the rest all had a process time of 30 days. The environmental temperature was maintained at 25.0±1.5 °C during the ALMT. Each experimental value is the average of two individual experimental results.

After the electrochemical process, the specimen was dry cut every 10 mm starting from the anode to the cathode. The Li^+, Na^+, and K^+ soluble content in the powder were extracted according to the AASHTO T260 experimental procedures and analyzed using IC.

3 RESULTS AND DISCUSSION

3.1 Migration behavior of cations during the ALMT

Figure 2 shows the typical curves, for the case of Mixture A2, between the cation concentration in the catholyte, the voltage and time during the ALMT. Using it, the migration behavior of Na^+ and K^+ under an electric field can be analyzed. The figure shows that three stages for Li^+ migration can be observed during the ALMT: non-steady state, transition, and steady state. During the non-steady state, Na^+ and K^+ in the mortar are migrating out of the specimen. At the same time, the Li^+ migrates to the saturated pores in the mortar, and have not yet passed through the specimen. The voltage first drops then increases. During the transitional stage, the foremost Li^+ has penetrated the specimen. The Li^+ in the specimen is not yet evenly distributed [6], while the Li^+ flux in the cathodic cell has increased, and the removal of Na^+ and K^+ is complete after the decreased flux (points A and B). The voltage reaches the peak value before complete Na^+ removal. During the steady state, after the removal of Na^+, the Li^+ concentration of pore solution in the mortar becomes steady, and the voltage decreases gradually. The flux of Li^+ transported into the catholyte is constant.

3.2 Changes in voltage and resistance during the ALMT

Figure 3 shows that the time required for reaching the peak value (t_p) decreases with the increase in V_f, while the peak value (V_{max}) increases with the increase in V_f. The result of t_p and V_{max} can be obtained from the curve during the transitional stage by regression analysis; the results are given in Table 3. When the aggregate volume fraction increases, the applied voltage also increases.

The system resistance can be obtained by dividing the voltage by the current (current density×cross section of specimen). Since this research applied a constant current density, the effect of the V_f on the system resistance-time curve is similar to the effect of the V_f on the voltage-time curve.

3.3 Effect of aggregate content on the migration behavior of Na^+ and K^+

From the Na^+ and K^+ concentration-time curve for the cathodic cell, the removal time of Na^+ and K^+ can be obtained; points A and B in Figure 2 are denoted by t_{Na} and t_K, respectively, in Table 4. The table shows that the removal time of Na^+ and K^+ will decrease with the increase in V_f. This result corresponds with the relationship between t_p and V_f. Since t_p is smaller than t_{Na}, t_p can act as a tool for evaluating the removal time of alkalis during the ALMT.

Table 4 shows that the removal time of K^+ is shorter than Na^+. Specifically, the removal percentage of Na^+ is 75.0-90.4%, while the removal percentage of K^+ is 68.9-79.0%. This result shows that the ability to remove Na^+ combined in the hydrated product is better than removing K^+. The w/c ratio of the matrix paste is reduced which tends to lower the matrix ions' migration. For the cement mortar, the volume of ITZ increases with the increase in V_f, so the decrement of the w/c ratio in the matrix paste increases. Therefore, the migration coefficient of the matrix ions will decrease. As shown in Table 4, the removed proportion of Na^+ and K^+ both decrease with the increase in V_f.

3.4 Effect of aggregate content on the migration behavior of Li^+

During the non-steady state, Li^+ has not yet reached the cathodic cell. Figure 4(b) shows the regression line for the Li^+ concentration-time curve during the transitional stage was produced to determine the time required for Li^+ to pass through the specimen:

$$C=at^b, \quad \text{for the transitional stage} \tag{1}$$

where C is the Li^+ concentration (mole/L) in the catholyte, t is the time for the electrochemical process (sec), a and b are experimental constants. This research has not adopted the method used to analyze the non-steady state migration coefficient of chloride. As IC is precise, we use Eq. (1) to calculate the time ($t_{0.1}$) corresponding to $C/C_0=0.1\%$ (C/C_0, Li^+ concentration in the catholyte/Li^+ concentration in the anolyte) as the time required for Li^+ to pass through the specimen, the results are given in Table 5. The table shows, for the cement mortar, the time $t_{0.1}$ will decrease with the increase in V_f.

During the steady state, the regression line for the curve during the steady state was produced (Figure 4(a)) to calculate the Li^+ migration rate (K) as follows:

$$C=Kt + c, \quad \text{for steady state} \tag{2}$$

where K (mole/L/s) is the slope of linear portion of the Li^+ concentration-time curve and c is experimental constant. This study has found that after the removal of Na^+, the migration of Li^+ begins to enter the steady state. While calculating the Li^+ steady state migration rate, the removal time of Na^+ was used as the beginning of Li^+ steady state migration. The steady state flux (J_s) can be calculated using steady state migration rate (K) × catholyte volume/specimen cross-section area. Table 5 shows, for the cement mortar, that the steady state flux will increase with the increase in V_f.

Migration coefficient of Li^+ during non-steady state

The non-steady state migration coefficient D_n of Li^+ can be calculated using a modified version of Fick's second law [9]:

$$\frac{dC}{dt} = D_n\left(\frac{d^2C}{dx^2} - \frac{|z|FE}{RT}\frac{dC}{dx}\right) \tag{3}$$

where C is the concentration of ions (mole/L) as a function of distance x, at any time t, D_n is the non-steady state migration coefficient (m^2/s), z is the electrical charge of Li^+, F is the Faraday constant (96500 C/mole), E is the strength of the electrical field between the anode and cathode (V/ m, in this research, E is the average strength of the electrical field during the non-steady state), R is the universal gas constant (8.3 J /mole/ K) and T is the absolute temperature (K). The initial condition is C=0 for x>0, t=0, the boundary condition is $C=C_0$ for $x=0$, $t>0$, and $C=0$ for x= infinite, t = large number. The analytical solution for Eq. (3) is given by:

$$C(x,t) = \frac{C_0}{2}\left[e^{ax}erfc\left(\frac{x+aD_nt}{2\sqrt{D_nt}}\right) + erfc\left(\frac{x-aD_nt}{2\sqrt{D_nt}}\right)\right] \tag{4}$$

where $a = \frac{|z|FE}{RT}$, C_0 is the Li^+ concentration (mole/L) in the cathodic cell, and *erfc* is the complementary error function.

From Eq. (4), D_n can be calculated as [9]

$$D_n = \frac{1}{a}\left[\frac{x-\alpha\sqrt{x}}{t}\right] \tag{5}$$

where $\alpha = 2\sqrt{\frac{1}{a}}erf^{-1}\left(1-\frac{2C}{C_0}\right)$, erf^{-1} is the inverse of the error function.

Use $t_{0.1}$ as the time needed by Li^+ to pass through the specimen. By substituting Eq. (5), D_n can be calculated, as shown in Table 5. The result show, for the cement mortar, the non-steady state migration coefficient will increase with the increase in V_f.

Flux and migration coefficient of Li^+ during steady state

There is no velocity of solution during the ALMT and, according to Kropp's research [10], while calculating the ionic flux, the diffusion effect produced by the concentration differential can be ignored. Therefore, the calculation of the steady state migration flux J_s of Li^+ can be simplified to:

$$J(x) = \frac{zF}{RT}D_sC_{up}\frac{\partial E_x}{\partial x} \tag{6}$$

where D_s is the steady state migration coefficient of ions (m^2/s), J_s is the steady state flux of ions ($mole/m^2/s$), and C_{up} is the concentration of ions in the upstream cell ($mole/m^3$).

Transposing Eq. (6) gives Eq. (7). Andrade [11] proposed that the solution of the steady state migration coefficient D_s of ions within concrete can be obtained by substituting the steady state flux J_s obtained from experiment into Eq. (7):

$$D_s = \frac{J_sRT}{zFC_{up}E} \tag{7}$$

Table 5 shows the J_s of the cement mortar increases with the increase in V_f. The D_s obtained from Eq. (7) decreases with increase in V_f when V_f is between 10-30%, while the D_s increases with increase in V_f when V_f is more than 30%.

Effect of aggregate contents on the Li^+ migration coefficient during steady state

(1) Dilution and tortuosity effects

If the bond between aggregate and paste is perfect, the mortar material will have a lesser migration coefficient than the matrix. Therefore, the dilution effect occurs because the migration coefficient of the aggregate is less than the paste [12]. In the ALMT, because the aggregate blocks the flow paths, the permeable area in a cross-section of mortar is reduced. The aggregate is relatively impermeable and a linear parallel Li^+ flow exists. By considering mortar as a two-phase composite material, for the dilution effect, the D_s of Li^+ of mortar can be expressed as [12]:

$$D_s=D_0(1-V_f) \tag{8}$$

where D_0 is the steady state migration coefficient of matrix.

The tortuosity effect occurs because the impermeability of the aggregate which forces flow around the aggregate. Thus, the length of flow paths increases and the flow rate reduces. Combining the tortuosity effect with the dilution effect, the Li^+ steady state migration coefficient can be expressed by Bruggeman equation [12]:

$$D_s=D_0(1-V_f)^{3/2} \tag{9}$$

This model assumes that the migration coefficient of matrix is constant as the spherical particles are added.

In Figure 5, the normalized Li^+ steady state migration coefficient of mortar with a 0.5 w/c ratio is plotted as a function of V_f, and is compared with the calculated results from Eq. (8) and (9). The normalized Li^+ migration coefficient, D_s/D_0, is defined as the ratio of the mortar Li^+ migration coefficient and the paste Li^+ migration coefficient. Comparing the experimental data with the theoretical results in Figure 5, the normalized Li^+ migration coefficient is influenced by the dilution effect and tortuosity effect, when V_f is less than 20%.

(2) ITZ and percolation effects

In this study, mortar is considered to be a three-phase composite material (paste, aggregate, and ITZ). The ITZ is characterized by a higher porosity and hence a lower density. The pores are generally larger than those found in the bulk paste. There is less C-S-H. There are large, oriented crystals of calcium hydroxide [4]. The ITZ, allowing accelerated ingress and movement of Li^+, will increase the Li^+ migration coefficient of mortar. The percolation effect occurs as the flow path connects the ITZs and increases the flow rate [12].

From Figure 5, the combination effect of ITZ and percolation occurs at V_f=30% for mortar with a 0.5 w/c ratio while the normalized Li^+ migration coefficients increase sharply as V_f rises over 30%. The combined effects of ITZ and percolation increase with the increase in V_f. This result implies that some percolation might be occurring as a result of the overlap of more porous ITZ regions.

3.5 Processes developing during the ALMT

As soon as the electricity was connected, the processes developing in the cell during the ALMT were: (1) Metal dissolution; and (2) Evolution of gases: as electrolysis of water, in both anolyte and catholyte, generating O_2 and H_2 [11]. The reactions occurring are:

anode: $2H_2O \rightarrow O_2 \uparrow +4H^+ + 4e^-$ (10)

cathode: $2H_2O + 2e^- \rightarrow H_2 \uparrow +2OH^-$ (11)

Using the accumulated amount of gas gathered from anolyte as an example, the result is shown in Figure 6. The relationship curves between the amount of the gathered gas and time for all mixtures are similar. The amount of gas and time exist in a positive linear relationship. The generated gases in the anolyte and catholyte are O_2 and H_2, respectively, examined by RGA.

3.6 Distribution of soluble cations in the specimen after the ALMT

Limiting the alkali content of cement or the total alkali content of concrete is an easy and effective strategy to limit ASR damage. ASTM limits the alkali content of cement to under 0.6 % Na_2O_{eq}.

Furthermore, the limit on the alkali content of concrete is specific to each region, thus, each country has different regulations. Hobbs [13] has pointed out that by using opal as aggregate, the concrete will not expand while its total alkali content is less than 2 kg/m^3.

Figure 7 shows that the free Na^+ and K^+ remaining in the mortar after the electrochemical process are both lower than the original contents in the mortar. After conversion into Na_2O_{eq}, it was found that the average residue alkali content of all experiments was less than 1.78 kg/m^3, lower than the total Na_2O_{eq} content before the electrochemical process, as shown in Table 6.

Figure 8 shows that the free Li^+ content in the mortar after the experiment gradually decreases from the anode to the cathode. Furthermore, the average free Li^+ impregnated into the mortar is 3.28, 3.38, 2.66, 2.72, 2.32, 2.32 and 1.99 kg/m^3 for Mixtures A0-A6 while there is little Na^+ and K^+ remaining within the specimen. Table 6 shows that the molar ratio of free Li/(Na + K) in the mortar is about 8.2-32.4 which far exceeds the suggested effective inhibiting value of 0.74 [2].

4 CONCLUSIONS

The following conclusions are drawn from this experiment:

(1) To remove Na^+ combined with the hydrated product is better than removing K^+. In this research, the ALMT removes 75.0-90.4% Na^+ and 68.9-79.0% K^+ and the removed proportion of the Na^+ and K^+ both decrease with the increase in V_f.

(2) Regarding the cement mortar, the non-steady state migration coefficient and the steady state flux increase with the increase in the volume fraction of fine aggregate.

(3) When V_f is less than 20% for mortar with a 0.5 w/c ratio, the normalized Li^+ migration coefficient is influenced by the dilution effect and tortuosity effect of fine aggregate. The combination effect of ITZ and percolation occurs at V_f=30%, and the effects increase with the increase in V_f.

(4) This research did not use corrodible electrodes, the generated gases in the anolyte and catholyte are O_2 and H_2, respectively.

(5) After the electrochemical process, the average residue Na_2O_{eq} of all experiments was less than 1.78 kg/m^3. The molar ratio of free Li/(Na + K) in the mortar is about 8.2-32.4.

5. ACKNOWLEDGEMENTS

The authors would like to thank the National Science Council of Taiwan for their financial support of this research under Contract No. NSC 100-2211-E-145-006-.

6 REFERENCES

[1] Chen DY (1999): Fundamental study using electrochemical technique to inhibit AAR. Master Thesis, Department of Civil Engineering, National Central University, Taiwain. (in Chinese)

[2] Liu CC (2003): Identify the reactivity of aggregates in Taiwan and using electrochemical techniques to mitigate expansion due to alkali-aggregate reaction in concrete. Ph.D. Thesis, Department of Civil Engineering, National Central University, Taiwain. (in Chinese)

[3] Yang CC (2006): On the relationship between pore structure and chloride diffusivity from accelerated chloride migration test in cement-based materials. Cement and Concrete Research (36/7): 1304-1311.

[4] Mindess S, Young JF, and Darwin D (2005): Concrete. Prentice Hall: 305.

[5] Yang CC (2005): Effect of the percolated interfacial transition zone on the chloride migration coefficient of cement-based materials. Materials Chemistry and Physics (91/3): 538-544.

[6] Tong L, and Gjorv OE (2001): Chloride diffusivity based on migration testing. Cement and Concrete Research (31/7): 973-982.

[7] Tian FZ (1999): Electrochemistry: basic principle and application. Five Continents Publishing House, Taipei: 23. (in Chinese)

[8] Delagrave A, Bigas JP, Olivier JP, Marchand J, and Pigeon M (1997): Influence of the interfacial zone on the chloride diffusivity of mortars. Advanced Cement Based Materials (5): 86-92.
[9] Yang CC, Cho SW, Chi JM, and Huang R (2003): An electrochemical method for accelerated chloride migration test in cement-based materials. Materials Chemistry and Physics (77/2): 461-469.
[10] Kropp J, and Hilsdorf HK (1995): Performance Criteria for Concrete Durability. RILEM REPORT 12, E & FN SPON: p. 244.
[11] Andrade C (1993): Calculation of chloride diffusion coefficients in concrete from ionic migration measurements. Cement and Concrete Research (23/3): 724-742.
[12] Yang CC, and Cho SW (2003): Influence of aggregate content on the migration coefficient of concrete materials using electrochemical method. Materials Chemistry and Physics (80/3): 752-757.
[13] Hobbs DW (1984): Expansion of concrete due to alkali-silica reaction. The Structural Engineer, Cement, Concrete, and Aggregate, England: 156.

TABLE 1: Chemical compositions of the cement. Unit: %

SiO_2	Al_2O_3	Fe_2O_3	CaO	MgO	SO_3	Na_2O	K_2O	Free lime	Total alkali as Na_2O_{eq}[a]
20.63	5.43	3.08	61.43	4.21	2.44	0.29	0.58	0.44	0.58

[a] $Na_2O_{eq}=Na_2O+0.658K_2O$

TABLE 2: Mixture design.

Mixture	Unit Content (kg/m^3)			V_f (%)
	Cement	Water	Fine Aggregate	
A0	1223	612	0	0
A1	1101	551	260	10
A2	979	489	520	20
A3	856	428	780	30
A4	734	367	1040	40
A5	612	306	1300	50
A6	489	245	1560	60

TABLE 3: The time required for reaching the peak value (t_p) and the peak value (V_{max}) during the ALMT.

Mixture	t_p (h)	V_{max} (V)
A0	428.4	5.79
A1	413.1	6.51
A2	291.1	7.31
A3	276.1	8.33
A4	181.0	9.22
A5	115.5	9.82
A6	84.0	9.96

TABLE 4: Results obtained from the Na^+ and K^+ concentration-time curve for the cathodic cell.

Mixture	t_{Na} (h)	t_K (h)	Removed Amount (mole)		Removed Proportion[a] (%)	
			Na^+	K^+	Na^+	K^+
A0	518.5	374.2	0.0219	0.0229	81.2	64.6
A1	528.5	376.2	0.0219	0.0225	90.4	70.5
A2	362.0	213.6	0.0194	0.0200	90.1	70.4
A3	334.4	230.5	0.0164	0.0166	86.8	66.7
A4	203.1	171.4	0.0135	0.0139	83.4	65.3
A5	157.6	159.5	0.0105	0.0106	78.2	60.0
A6	144.3	143.8	0.0081	0.0083	75.0	58.4

Note: [a] The removed proportion of the Na^+ and K^+ is obtained by dividing the removed amount by the total amount in the corresponding mixture. Mixtures A0-A6, the total amounts of Na^+ in a mortar are: 0270, 0.0243, 0.0216, 0.0189, 0.0162, 0.0135, and 0.0108 mole, respectively.

TABLE 5: The migration coefficients of Li^+ during non-steady and steady state.					
Mixture	Non-Steady State		Steady State		
	$t_{0.1}$ (h)	D_n ($\times 10^{-12}$ m^2/s)	J_s($\times 10^{-6}$ mole /m^2/s)	D_s($\times 10^{-13}$ m^2/s)	Normalized Migration Coefficient [a]
A0	395.4	2.07	1.40	2.18	1.00
A1	415.5	1.78	1.26	1.78	0.82
A2	310.9	2.21	1.32	1.63	0.75
A3	295.6	2.05	1.38	1.53	0.71
A4	214.9	2.57	2.27	2.39	1.10
A5	162.3	3.24	3.24	3.39	1.56
A6	113.9	4.46	4.31	4.44	2.04

Note: [a] The normalized Li^+ migration coefficient, D_s/D_0, is defined as the ratio of the mortar Li^+ migration coefficient and the paste Li^+ migration coefficient.

TABLE 6: Changes in alkali contents in the mortar before and after the ALMT.			
Mixture	Before the ALMT Experiment	After the ALMT Experiment	
	Total Na_2O_{eq} (kg/m^3)	Average Residual Na_2O_{eq} (kg/m^3)	Li/(Na + K) Molar Ratio
A0	8.21	1.15	29.8
A1	7.39	0.59	32.4
A2	6.58	1.43	16.7
A3	5.75	1.51	11.2
A4	4.93	1.78	7.2
A5	4.11	1.52	8.7
A6	3.28	1.41	8.2

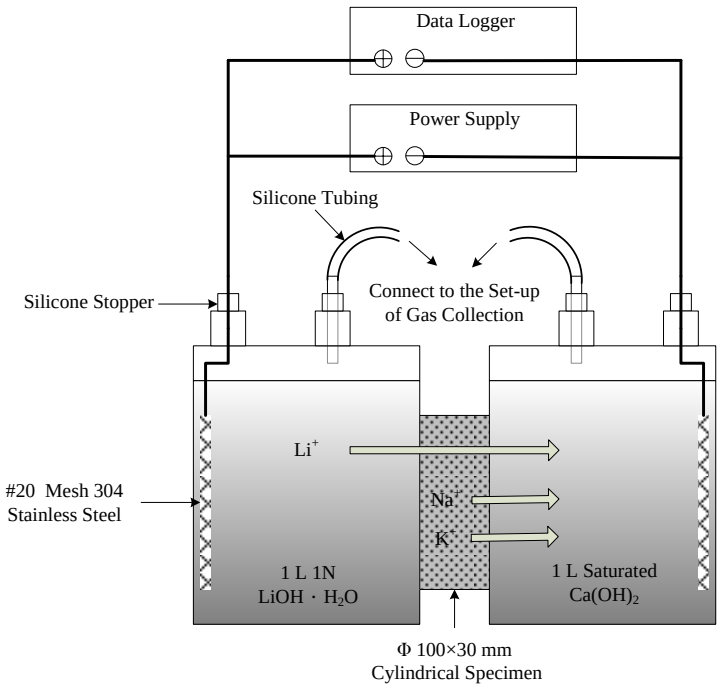

FIGURE 1: Schematic diagram of the ALMT set-up.

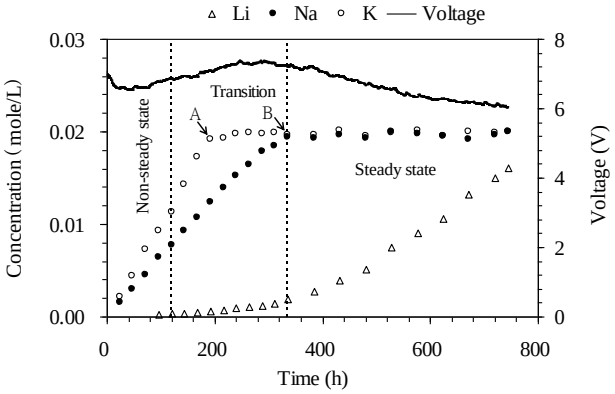

FIGURE 2: Typical curves between the cation concentration in the catholyte.

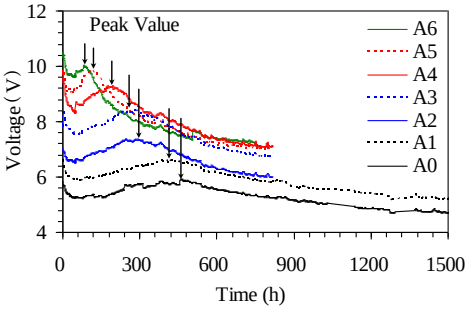

FIGURE 3: Changes in voltage during the ALMT.

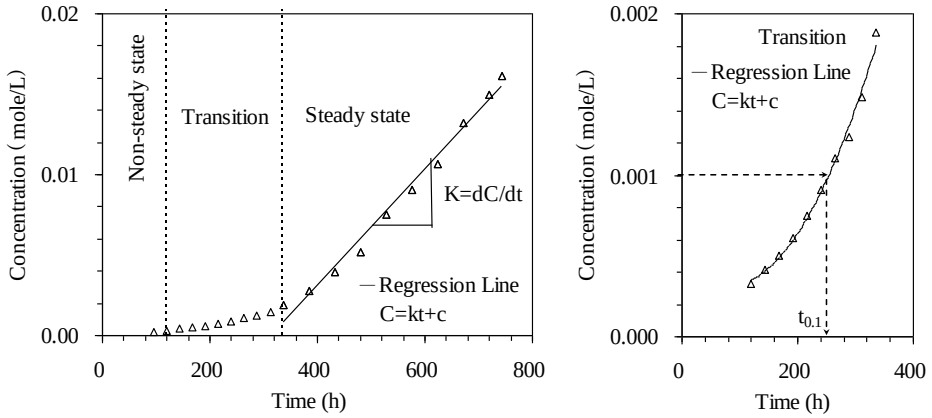

(a) (b)

FIGURE 4: (a) Changes in the Li^+ concentration in the catholyte and (b) changes of concentration during transitional stage.

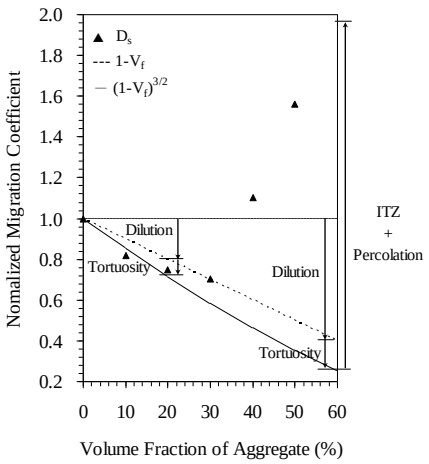

FIGURE 5: Li^+ steady state migration coefficient vs. volume fraction of aggregate for mortar with a 0.5.

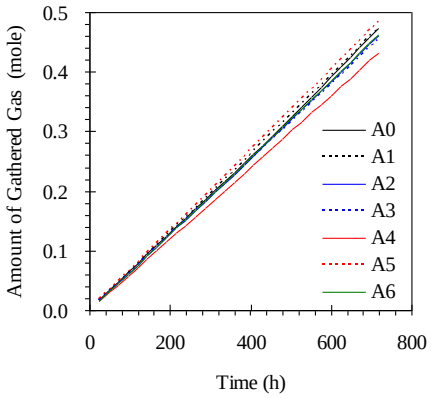

FIGURE 6: Curves between the amount of the gathered gas in the anodic cell and time during the ALMT.

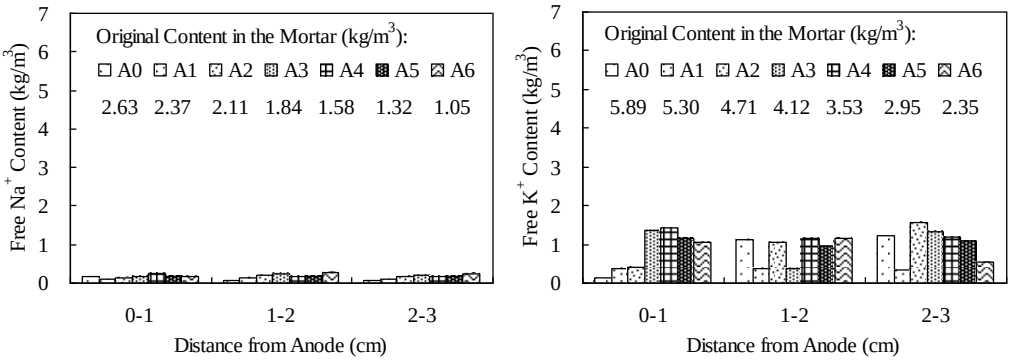

(a) (b)

FIGURE 7: Free Na^+ and K^+ contents in the mortar after electrochemical processing.

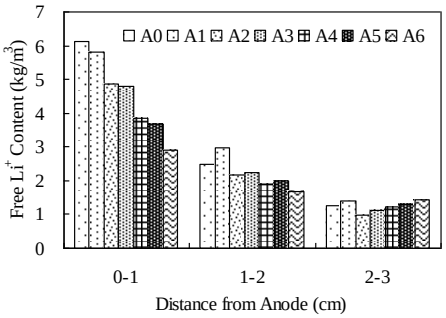

FIGURE 8: Free Li^+ content in the mortar after electrochemical processing.